Biomaterials 34 (2013) 5172–5180

Contents lists available at SciVerse ScienceDirect

Biomaterials

journal homepage: www.elsevier.com/locate/biomaterials

Multifactorial diagnostic NIR imaging of CCK2R expressing tumors

Susanne Kossatz [a,*], Martin Béhé [b], Rosalba Mansi [c], Dieter Saur [d], Peter Czerney [e], Werner A. Kaiser [f], Ingrid Hilger [a,**]

[a] Dept. of Experimental Radiology, Institute of Diagnostic and Interventional Radiology I, Jena University Hospital, Friedrich Schiller University Jena, Erlanger Allee 101, D-07747 Jena, Germany
[b] Paul Scherrer Institute, Center for Radiopharmaceutical Sciences ETH-PSI-USZ, Villigen-PSI, Switzerland
[c] Institute for Nuclear Medicine, Freiburg, Germany
[d] II. Medizinische Klinik, Technical University of Munich, Munich, Germany
[e] Dyomics GmbH, Jena, Germany
[f] Institute of Diagnostic and Interventional Radiology I, Jena University Hospital, Friedrich Schiller University Jena, Jena, Germany

ARTICLE INFO

Article history:
Received 21 January 2013
Accepted 23 March 2013
Available online 13 April 2013

Keywords:
Multifactorial imaging
CCK2-receptor
Minigastrin
Tumor metabolism
Optical peptide probes
In vivo optical imaging

ABSTRACT

Optical imaging-based diagnostics identify malignancies based on molecular changes instead of morphological criteria in a non-invasive, irradiation free process. The aim of this study was to improve imaging efficiency by the development of a new Cholecystokinin-2-receptor targeted fluorescent peptide that matches the clinical needs regarding biodistribution and pharmacokinetics while displaying superior target specificity. Furthermore we performed multifactorial imaging of Cholecystokinin-2-receptor and tumor metabolism, since simultaneous targeting of various tumor biomarkers could intensely increase tumor identification and characterization. Affinity and specificity of the fluorescent Cholecystokinin-2-receptor targeted minigastrin (dQ-MG-754) were tested *in vitro*. We conducted *in vivo* imaging of the dQ-MG-754 probe alone and in a multifactorial approach with a GLUT-1 targeted probe (IR800 2-DG) on subcutaneous xenograft bearing athymic nude mice up to 24 h after intravenous injection ($n = 5$/group), followed by *ex vivo* biodistribution analysis and histological examination. We found specific, high affinity binding (Kd = 1.77 nM ± 0.6 nM) of dQ-MG-754 to Cholecystokinin-2-receptor expressing cells and xenografts as well as favorable pharmacokinetics for fluorescence-guided endoscopy. We successfully performed multifactorial imaging for the simultaneous detection of the Cholecystokinin-2-receptor and GLUT-1 targeted probe. Prominent differences in uptake patterns of the two contrast agents could be detected. The results were validated by histological examinations. The multifactorial imaging approach presented in this study could facilitate cancer detection in diagnostic imaging and intraoperative and endoscopic applications. Especially the dQ-MG-754 probe bears great potential for translation to clinical endoscopy imaging, because it combines specific high affinity binding with renal elimination and a favorable biodistribution.

1. Introduction

Optical imaging is rapidly advancing toward clinical application for early cancer detection and intraoperative imaging [1]. Beyond the recognition of only visible morphological changes, it enables the non-invasive detection of molecular changes in malignant cells. In this context, fluorescent probes have been developed for a wide range of tumor specific targets, mostly addressing only one specific marker in each approach. Considering that pathobiological mechanisms are very complex, the visualization of several tumor markers at a time could fundamentally improve tumor detection and characterization. The implementation of such multifactorial approaches, for example in fluorescence-guided endoscopy, could foster early identification of malignant cells [2] and prognosis by assessment of their developmental stage.

Particularly in relation to the identification of colon cancers, the second leading cause of death in men and women in developed countries [3,4], small or flat lesions are often missed in conventional endoscopic screening [5]. In these cancers the cholecystokinin-2-receptor (CCK2R), is one of the receptors which is overexpressed early in the transition from adenoma-carcinoma, allowing for early discovery of malignant lesions [6]. The receptor

* Corresponding author. Tel.: +49 3641 9325924; fax: +49 3641 9325922.
** Corresponding author. Tel.: +49 3641 9325921; fax: +49 3641 9325922.
E-mail addresses: susanne.kossatz@med.uni-jena.de (S. Kossatz), ingrid.hilger@med.uni-jena.de (I. Hilger).

0142-9612
http://dx.doi.org/10.1016/j.biomaterials.2013.03.073

has been shown to be involved in tumorigenesis, progression and invasiveness of various tumor types [7–10] by CCK2R dependent activation of several tumorigenic pathways [11–14]. The expression of the receptor in normal tissue is primarily located in the central nervous system and in the stomach, whereas it has been reported that in the normal colon the CCK2R is not expressed [6].

In 1999, a short 7 amino acid sequence called "minigastrin" has been selected from a large screening for CCK2R binding peptides [15]. Since then several chelate based minigastrin analogs with high target affinity, fast kinetics and renal elimination have been developed to improve tumor targeting properties [16,17]. Replacement of the radioactive moiety with a near infrared fluorophore makes these substances available for fluorescence endoscopy or intraoperative imaging [18]. However, improved fluorescent minigastrins with suitable pharmacokinetics and superior target affinity remain to be identified [19].

In terms of multifactorial imaging, an important functional change in cancer development is acceleration of glucose metabolism [20]. The observations of prevalent GLUT-1 overexpression in tumors and correlations to poor prognosis and chemotherapy resistance are already being widely exploited in ^{18}F-FDG nuclear imaging of tumors [21]. Translation of GLUT-1 imaging to optical imaging led to the development of a commercially available 2-deoxy-D-glucose (2-DG), where the radioligand was replaced by the near infrared dye IRDye 800CW [22]. So far, reports on the reliability of the probe have been somewhat contradictory. Whereas some research reports proposed a specific binding mechanism [22,23], another research proposed an EPR effect dependent accumulation [24].

Here, we explored the feasibility of multifactorial NIR optical imaging with a CCK2R targeted peptide and a fluorescent 2-DG probe. We aimed at synthesizing a CCK2R targeted probe by linking a NIRF dye via a hydrophilic linker to a high-affinity peptide to obtain pharmacokinetic properties fitted to prospective clinical endoscopic imaging. Our hypothesis was that probe properties could be selectively modulated to increase affinity, specificity, and renal elimination. To show the feasibility of the multispectral approach, we explored and characterized differences in uptake patterns of the two contrast agents in subcutaneous xenografts *in vivo*. We propose that the approach described here could foster the development of multifactorial approaches in optical imaging.

2. Material and methods

2.1. Cell lines

A431/CCK2R and A431/WT, human epidermoid carcinoma cells were a gift from Dr. Luigi Aloj (Department of Nuclear Medicine, Instituto Nazionale Tumouri, Fondazione "G. Pascale", Naples, Italy). The cells were stably transfected with either the CCK2-Receptor (A431/CCK2R) or with empty vector (A431/WT) [25]. Authenticity of the cells was confirmed by DSMZ (Deutsche Sammlung für Mikroorganismen und Zellkulturen) in 2012. HT-29 and LS174T colorectal adenocarcinoma cell lines were obtained from DSMZ and CLS. All cell lines were grown in a monolayer culture at 37 °C in a 5% CO_2 humidified atmosphere. They were maintained in D-MEM medium with 10% (v/v) FBS (both Gibco® (Invitrogen)) and passaged regularly at 70–80% confluency.

2.2. Animals

Female athymic nude mice (Hsd:Athymic Nude-Foxn1^{nu} nu/nu; Harlan Laboratories) were housed under standard conditions with water and food ad libitum. Mice were maintained under a low-pheophorbide diet (C 1039; Altromin) to reduce tissue autofluorescence. All procedures were approved by the regional animal committee and were in accordance with international guidelines on the ethical use of animals. Throughout all procedures, animals were anesthetized with 2% isoflurane. To implement subcutaneous xenografts, 5×10^5 cells (A431/CCK2R and A431/WT) or 2×10^6 cell (HT-29 and LS174T) were dispensed in Matrigel™ (BD Biosciences) and injected into right (A431/CCK2R cells) and left (A431/WT cells) flank or the middle of the back (HT-29 and LS174T) of 8–12 weeks old animals 10–15 days before *in vivo* imaging.

2.3. Target expression in A431/CCK2R und A431/WT cells

RNA isolation from 5×10^6 cells with TRIzol® (Invitrogen) was performed according to standard protocol [26]. After cDNA synthesis with the QuantiTect RT Kit (Qiagen), SYBR® green qRT-PCR was performed on a RotorGene Q (Qiagen). Reactions consisted of RotorGene™ SYBR® Green Mastermix (Qiagen), forward/reverse Primer (see Fig. S1) DEPC water and cDNA. Samples were denaturized at 95 °C and amplification was carried out over 40 cycles of 5 s 95 °C and 10 s 60 °C. CCK2R gene expression was relatively quantified using the ΔΔCt method.

2.4. Synthesis of CCK2R targeted probe "dQ-MG-754" with improved pharmacokinetics

We designed a NIRF peptide probe for CCK2R imaging. The hemicyanine fluorescent dye DY-754 (Dyomics) was used as signaling moiety of the probe construct. This dye was selected out of six different hemicyanine NIR dyes (DY-676, DY-677, DY-678, DY-751, DY-752 and DY-754) due to its low nonspecific binding to the gastrointestinal tract and renal elimination pattern (see Supplementary Figs. 1 and 2). Then, a *N*-Hydroxysuccinimide-ester of DY-754 was N-terminally coupled to the minigastrin peptide analog with the sequence H_2N-$(DGln)_6$-Ala-Tyr-Gly-Trp-Met-Asp-Phe-amid [27]. The probe construct was named "dQ-MG-754". Peptide synthesis, dye coupling and HPLC purification were carried out by Peptide Specialty Laboratories (PSL).

2.5. In vitro dQ-MG-754 probe uptake into A431/CCK2R and A431/WT cells

For determination of probe uptake, cells were seeded into chamber slides and incubated with 5 nM dQ-MG-754 in culture medium at 4 °C and 37 °C for 30 min. Cell membranes were stained with Alexa-555 conjugated wheat germ agglutinin (WGA-555; Invitrogen) and subsequently fixated with 4% paraformaldehyde (Roth). Cells were mounted with PermaFluor® mounting medium (ThermoFischer) containing Hoechst 33258 DNA stain (Applichem). Using a laser scanning microscope (LSM 510, Zeiss), cell nuclei were visualized with a 405 nm laser diode and a 420–480 nm bandpass filter. For cell membranes, a 543 nm HeNe laser and a 550–615 nm bandpass filter were applied, fluorescence of dQ-MG-754 was excited with a 633 Argon Laser and emission was detected with a 650 nm longpass filter. Binding specificity was controlled by incubation of cells with either the probe together with 10-fold excess unlabeled peptide or an equimolar concentration of DY-754.

Furthermore interactions of dQ-MG-754 probe with tumor (A431/CCK2R and A431/WT), endothelial (HMEC-1) and kidney cells (HEK293) were investigated by the means of real time impedance measurement (xCELLigence, Roche). Therefore, cells were incubated with 50 μM probe over a period of 96 h. Change of impedance by proliferation activities of cells was measured as "Cell Index" [28] and normalized to untreated cells.

2.6. Fluorescence based determination of binding affinity

To obtain a saturation binding curve, 2×10^6 A431/CCK2R cells were incubated with serial dilutions from 0.1 to 50 nM of dQ-MG-754 for 5 min at room temperature to measure total probe binding. To determine nonspecific binding, the same probe concentrations were used in presence of 100-fold excess unlabeled peptide (D-Leu-minigastrin, Bachem). After centrifugation cell pellets were immediately imaged with the small animal imaging system Maestro™ (CRi). A region of interest (ROI) was assigned to each cell pellet in order to measure fluorescence intensity semi-quantitatively. Fluorescence intensities were described as average signal (scaled counts/s). This value represents count levels after scaling for exposure time, camera gain, binning and bit depth, hence measurements are comparable among each other. Binding curves and dissociation constants were determined using Graphpad Prism 5. Specific binding was assessed by subtracting nonspecific binding signal from total binding signal.

Determination of the Ki value was carried out by preincubating cells with increasing concentrations of unlabeled peptide from 0.1 to 2000 nM directly before adding a fixed probe concentration of 2 nM to all samples. Thereafter, the same procedure as described above was followed.

2.7. In vivo imaging of CCK2R expression and elevated rate of glycolysis

When subcutaneous xenografts reached a diameter of 5–7 mm, *in vivo* imaging was initiated by tail vain injection of the respective contrast agent. For solitary imaging of dQ-MG-754, we injected 108 nmol/kg. To control signal specificity, animals received probe together with a 10-fold excess of unlabeled D-Leu-minigastrin or the native fluorophore (108 nmol/kg of DY-754). For multifactorial imaging of CCK2R expression and elevated rate of glycolysis we injected 108 nmol/kg dQ-MG-754 and 608 nmol/kg IRDye 800CW 2-DG (short: IR800 2-DG; LI-COR) simultaneously.

At defined time points after injection, animals were imaged in the Maestro® using filters for excitation (670–710 nm) and emission (longpass > 750 nm). Semiquantitative analysis of fluorescence intensities was carried out as described above. Each contrast agent was analyzed separately for its distinct fluorescence spectrum after subtraction of autofluorescence. A tumor to background ratio (TBR)

as measure of contrast was calculated by dividing the average fluorescence signals of a defined ROI in the tumor area by a ROI of normal tissue between the animal's ears. A TBR of ≥3 was considered to be a contrast suitable for unequivocal tumor detection.

2.8. Ex vivo determination of improved pharmacokinetic properties of dQ-MG-754

Animals were sacrificed 8 h after injection and fluorescence intensities of the organs, GI tract A431/CCK2R and A431/WT tumors were determined with the Maestro™. We used the same protocol as described above to measure and compare organ fluorescence of animals injected with probe, block, DY-754 and control animals (nothing injected). Excised tumors were processed for histological analysis.

2.9. Analysis of probe distribution in tumor tissue ex vivo

To determine the distribution and localization of dQ-MG-754 and IR800 2-DG within the tumor tissue, we recorded macroscopic scans of 30 μm tumor cryosections (Odyssey, LI-COR). Autofluorescence was determined at 700 nm and probe fluorescence at 800 nm.

2.10. Determination of xenograft vascularization

We used the Chalkley counting method to estimate tumor vascularity as recommended in an international consensus [29]. Detailed description of the method can be found elsewhere [30,31]. Vessels were stained with CD31. Briefly, fixed cryosections were blocked with Biotin Blocking System (Dako), according to the manufacturers' recommendations. Primary antibody (rat anti mouse-CD31, MEC13.3, 0.625 mg/mL, BD Biosciences) incubation for 1 h was followed by secondary antibody (biotinylated IgG2a 0.25 mg/mL, BD Biosciences) for 45 min, both at room temperature. The Dako REAL™ Detection System (Dako) was used for streptavidin-biotin detection. Between these steps slides were washed with TBS-T buffer. Cell nuclei were counterstained with Mayer's hematoxylin (Fluka/Sigma–Aldrich) and mounted with gelatine (SERVA Electrophoresis).

2.11. Immunohistochemical validation of target expression in xenografts (GLUT-1, CCK2R)

For staining of GLUT-1 receptor, paraffin sections were deparaffinized, followed by antigen demasking at 98 °C for 10 min in EDTA buffer pH 9.0. Slides were blocked with the avidin/biotin blocking system (Dako) and 5% goat serum. Thereafter primary antibody (polyclonal rabbit anti-human GLUT1, NB110-39112, 4 μg/ml) was added for 1 h at room temperature. Secondary antibody incubation and streptavidin-biotin detection were carried out with the Dako Kit 5005 (Dako) according to the manufacturers' recommendations. Between all steps slides were washed with TBS-T buffer.

For immunodetection of CCK2R expression, formalin-fixed paraffin-embedded tissue sections were dewaxed and placed in a microwave (10 min, 600 W) to recover antigens before incubation with the CCK2R antibody (1:300; PAB6797, Abnova), followed by secondary biotinylated antibody (Vector Laboratories). Peroxidase conjugated streptavidin was used with 3,3′-diaminobenzidine tetrahydrochloride (DAB, Sigma–Aldrich) as chromogen for detection. Cell nuclei were counterstained with Mayer's hematoxylin (Fluka/Sigma–Aldrich) and mounted with gelatine (SERVA Electrophoresis).

2.12. Statistics

To determine the level of significance, student's *t*-test was used, if normality and equal variance tests were passed. Otherwise Mann-Whitney-Rank Sum Test was applied. All experiments were done at least in triplicate and experimental *in vivo* groups consisted of 5 or more animals.

3. Results

3.1. Features of the probes and target cells

The CCK2R targeted probe dQ-MG-754 (Fig. 1A) featured near-infrared excitation and emission spectra (Fig. 1B), while exhibiting low molecular weight of $M = 2604$ g/mol and a strongly negative log *P* value, which is an indicator of high hydrophilicity. Basic spectroscopic and photophysical parameters are listed in Fig. 1C.

The dye component of the probe, DY-754, was chosen from preliminary experiments, where we comparatively evaluated two groups of three NIR dyes (Suppl. Fig. S1A+B). The dyes with four

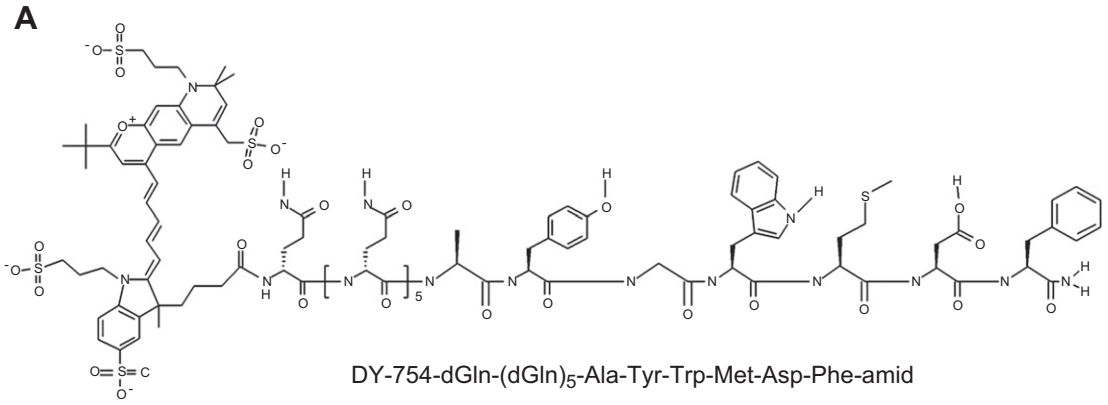

C

Probe characteristics			
Excitation	748 nm	Emission	774 nm
MW	2604 g/mol	Log (P)	-2.949
Quantum Yield	13.1%	Photo-stability	31.1 min
Fluorescence lifetime	720 ps		

Fig. 1. CCK2R targeted probe design and target expression. (A) Chemical structure of dQ-MG-754, composed of a hemicyanine fluorescent dye and a dQ_6-minigastrin peptide, (B) Spectroscopic features of the probe, (C) Photophysical and spectroscopic probe properties are presented in the table. Quantum yield was measured with a Hamamatsu C9920-2 Total Photoluminescence Quantum Yield Measurement System at 700 nm. Photostability was determined in water during white light exposure.

sulfonate groups (DY-678 and DY-754) showed extremely low unspecific binding to non-cancerous tissue of the gastrointestinal tract compared to the dyes with two or three sulfonate groups (Suppl. Fig. S1C+D). Furthermore, we demonstrated that DY-754 was the only dye to show almost exclusive clearance through the kidneys in mice *in vivo* (Suppl. Fig. S2A+B). DY-751 and DY-752 were partly or completely subject to hepatobiliary elimination, with resulting intense fluorescence in the intestine (Suppl. Fig. S2C). qPCR confirmed that only the transfected A431/CCK2R cells expressed high mRNA levels of CCK2R (Suppl. Fig. S3).

3.2. Probe binding to CCK2R expressing cells

Microscopic analysis showed strong binding of the dQ-MG-754 probe to A431/CCK2R cells. Internalization was observed at 37 °C, but not at 4 °C (Fig. 2A). The probe bound A431/CCK2R cells but not A431/WT cells (Fig. 2B-I and B-II). Binding was strongly inhibited by preincubation with an excess of unlabeled peptide, which blocks the specific binding sites (Fig. 2B-III). The dye DY-754 alone displayed no binding to both tested cell lines (Fig. 2B-IV). Furthermore we could show that binding of dQ-MG-754 also occurred to HT-29 and LS174T colorectal adenocarcinoma cells, but not to A431/WT and HMEC-1 cells (Suppl. Fig. 5A–B).

The saturation binding assay demonstrated high binding affinity to receptor expressing cells, with a K_d value of 1.77 nM ± 0.6 nM (Fig. 2C). The competitive displacement cell binding assay with unlabeled D-Leu-minigastrin as competitor revealed a *Ki* value of 7.6 nM ± 0.04 nM (Fig. 2C). Incubation of tumor and non-tumor cell lines with dQ-MG-754 showed no negative influence on cell viability. A transient increase in proliferation was observed in A431/CCK2R cells (Fig. 2D).

3.3. In vivo imaging of CCK2R expressing tumors

After intravenous probe injection, we observed a fast, high contrast and long lasting accumulation in tumors expressing CCK2R (Fig. 3). A much weaker accumulation occurred in A431/WT xenografts and background tissue. The tumor to background ratios (TBR) in A431/CCK2R xenografts after probe application exhibited values ≥3 from 2 h to 24 h after probe application (Fig. 3). Blocking of specific binding sites by 10-fold excess of competing unlabeled peptide reduced probe accumulation in A431/CCK2R tumors by 53%

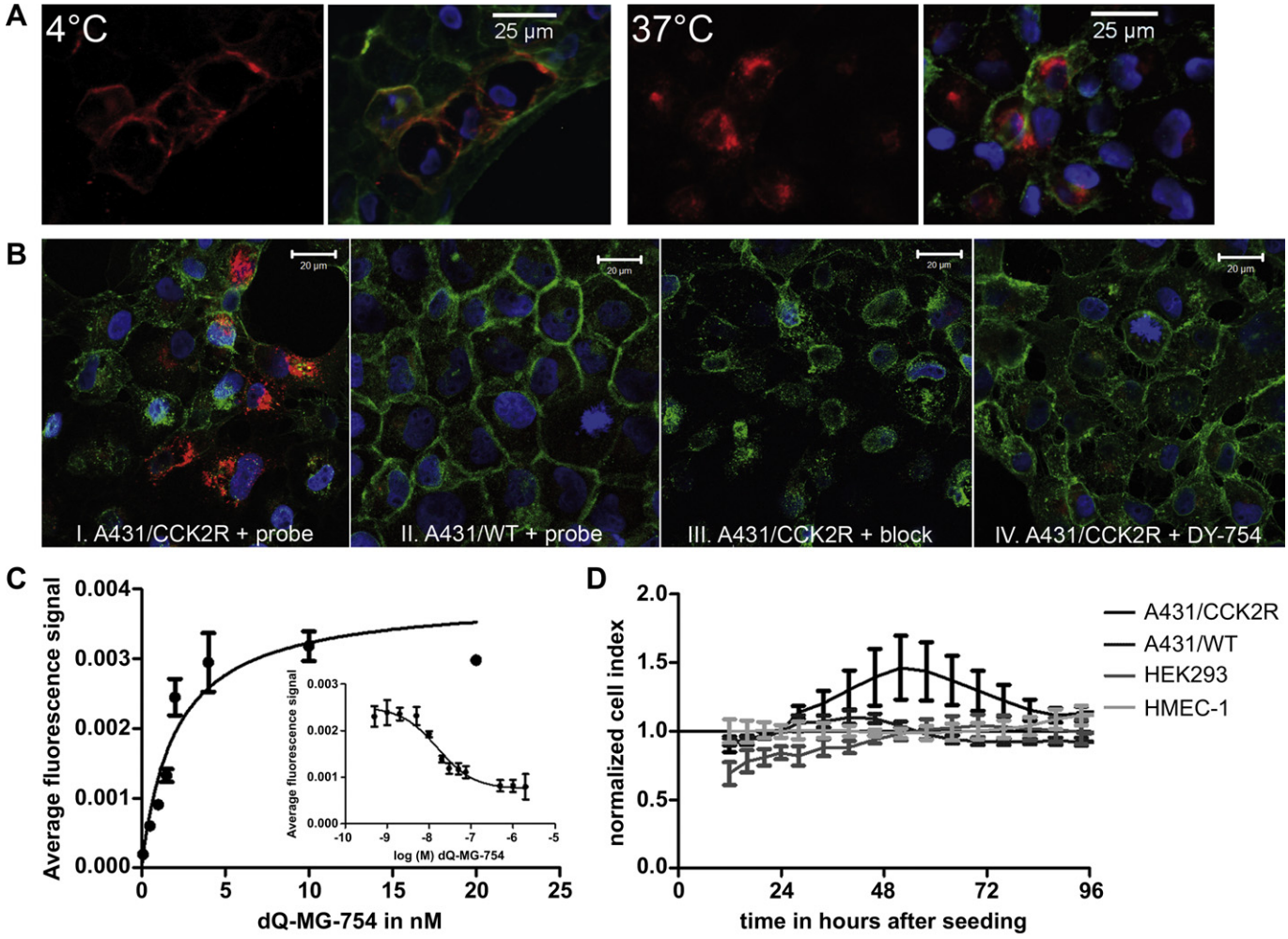

Fig. 2. *In vitro* characterization reveals a specific cell uptake of the dQ-MG-754 probe and cytotoxic harmlessness. A) dQ-MG-754 probe binding (red) was located at the cell membrane (green) at 4 °C and close to the nucleus (blue) at 37 °C. B) dQ-MG-754 probe uptake occurs only into receptor expressing (I) and not in non-expressing cells (II) after incubation at 37 °C. Incubation with excess unlabeled D-Leu-minigastrin (III) and free DY-754 (IV) was carried out to control for specificity of probe uptake. Blue: DNA stain Hoechst 33258, Green: cell membranes stain WGA-Alexa 555, Red: dQ-MG-754. C) Saturation binding curve of dQ-MG-754 to A431/CCK2R cells reveals a dissociation constant (*Kd*) of 1.77 nM ± 0.6 nM. The graph insert shows a *Ki* value of 7.6 nM ± 0.04 nM. D) Incubation of tumor and non-tumor cell lines with 50 µM dQ-MG-754 showed no negative influence on cell viability. A transient increase in proliferation was observed in A431/CCK2R cells. The cell index [28] is presented relative to untreated cells. All graphs display means of $n = 3 \pm$ SEM.

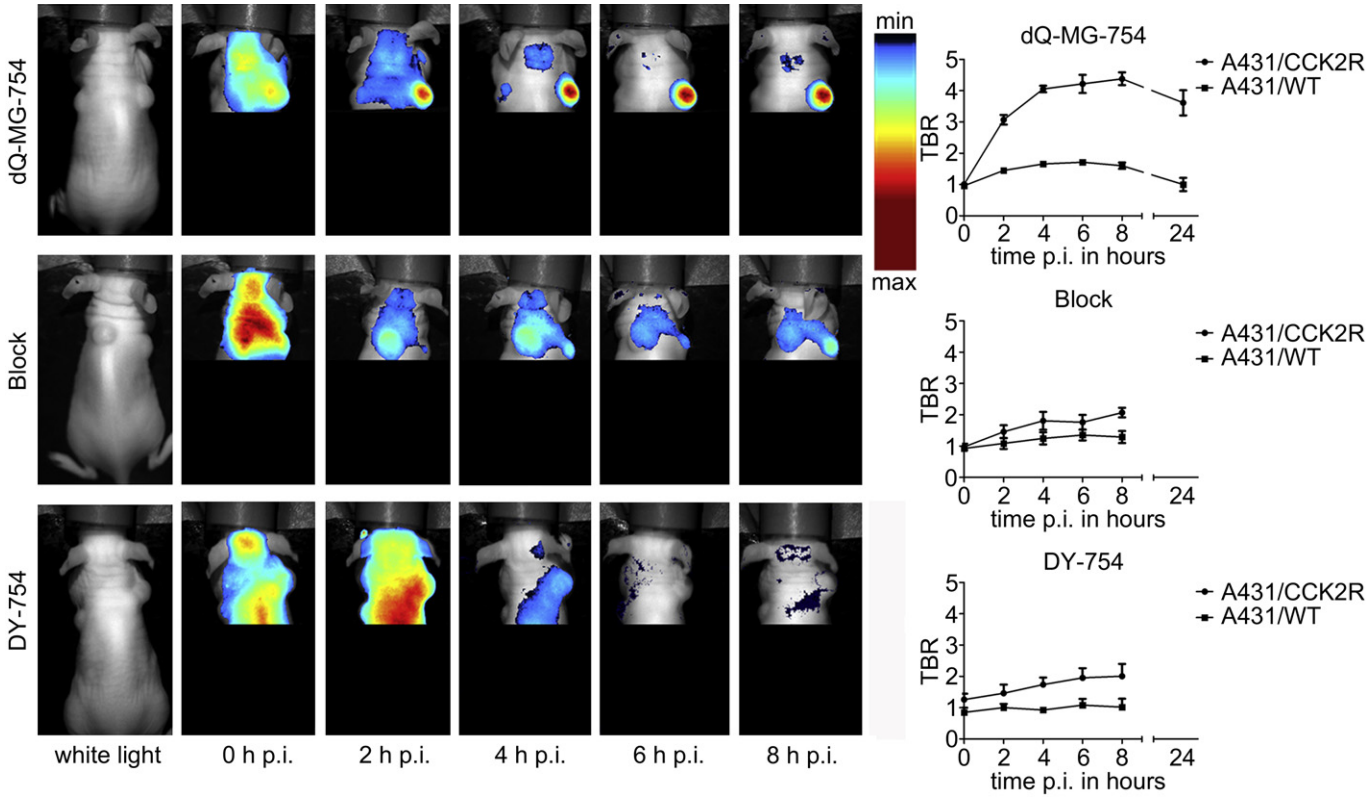

Fig. 3. dQ-MG-754 probe accumulates specifically in A431/CCK2R xenografts. NIR fluorescence reflectance images of CCK2R expression in an A431/CCK2R (right flank) and A431/WT (left flank) xenograft model. The left panel displays representative intensity scaled fluorescence images for each experimental group at indicated time points after probe injection. "Tumor to background ratios" (TBRs) in the right panel represent relative tumor uptake of each group. Error bars indicate SEM ($n = 5$; except dQ-MG-754 group 0–8 h: $n = 12$). Images were acquired with the Maestro™.

8 h p.i. ($p < 0.01$). We detected no specific tumor uptake for DY-754. Analysis of probe kinetics showed that the fluorescence signal peaked directly after application with subsequent gradual washout (Suppl. Fig. S4). We observed a significantly reduced washout of dQ-MG-754 probe in A431/CCK2R tumors compared to the blocked ones ($p \leq 0.05$) between 2 and 8 h p.i.. In contrast, the washout in A431/WT tumors could not be delayed.

To secure that the xenograft models featured comparable drug delivery characteristics we quantified tumor vascularization. We found both xenograft models well vascularized, however the A431/CCK2R tumors (8.04 ± 1.77) presented an elevated chalkley count compared to A431/WT tumors (6.9 ± 1.06) (Fig. 4). Therefore drug delivery is essentially comparable, but the differences in vascularization could account for slightly higher unspecific accumulation in the receptor expressing tumors.

We could corroborate a favorable probe biodistribution, in terms of prospective intraoperative and endoscopic imaging, by examination of organ fluorescence 8 h p.i. (Fig. 5A). We observed high kidney fluorescence and strong fluorescence signal which correlated with the anatomical localization of the bladder. These findings verified that the probe was cleared through the kidneys and excreted via the bladder in a manner comparable to DY-754 (Fig. 5B). Only a small proportion was processed through the liver, resulting in low liver fluorescence. Other organs did not exhibit notable fluorescence signals. Interestingly, there were no detectable fluorescence signals in the gastrointestinal tract, which could potentially disturb endoscopic imaging.

The dQ-MG-754 probe was also able to image physiological CCK2R expression in xenografts derived from colorectal adenocarcinoma cells HT-29 and LS174T. Probe accumulation in tumor tissue was fast and high tumor to background contrasts were reached between 1 and 24 h p.i. (Suppl. Fig. 5C). For HT-29 tumors, 24 h p.i. we found a TBR of 4.8 ± 0.4 and for LS174T the TBR was 3.8 ± 0.4. To determine the specificity of this uptake we performed a blocking experiment as described above. Blocking experiments led to a 49% lower TBR at 24 h p.i. in HT-29 tumors (2.4 ± 0.5, $p = 0.009$) and to a 41% lower TBR in LS174T xenografts (2.2 ± 0.1, $p = 0.02$) (Suppl. Fig. 5D).

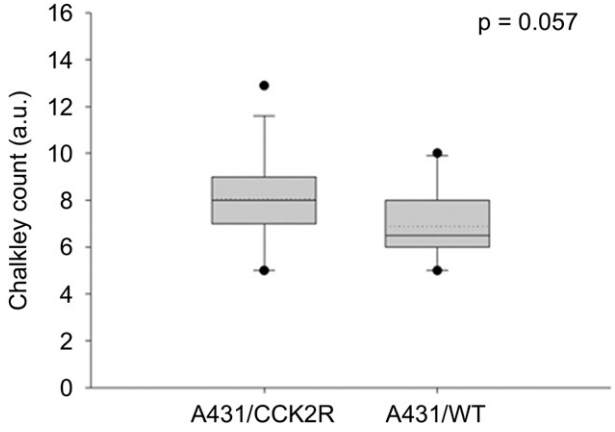

Fig. 4. Average signal intensity of tumors correlates with angiogenesis. Vessel density as determined by Chalkley count shows a tendency towards higher vascularization in A431/CCK2R xenografts compared to A431/WT xenografts ($p = 0.057$). Chalkley count units are related to the mean number of points on a Chalkley 25-point eyepiece graticule that overlap with vessels in vascular hotspots. Detailed description of the method can be found in the literature [29,30].

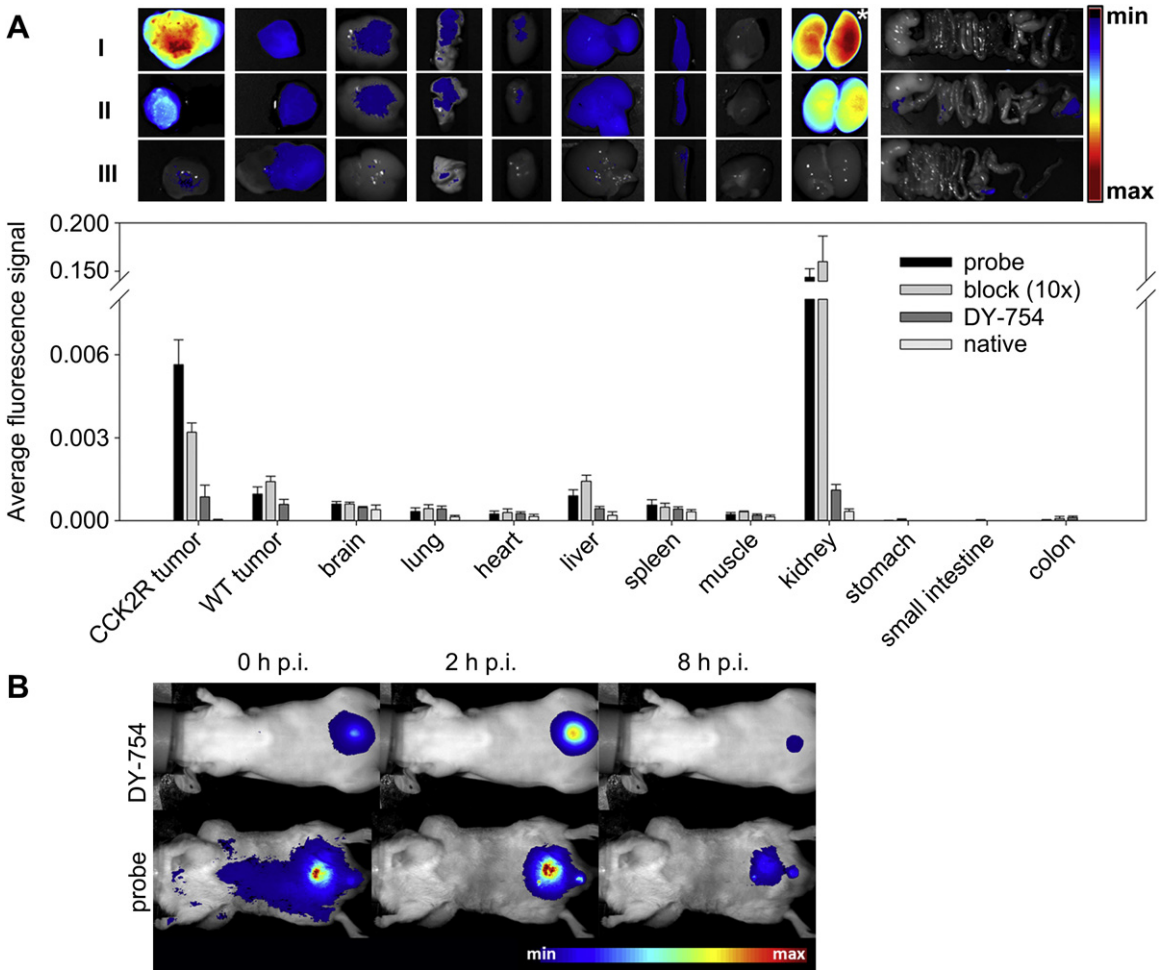

Fig. 5. Biodistribution of dQ-MG-754 shows high tumor uptake and kidney retention. Biodistribution analysis 8 h p.i. revealed specific tumor uptake of dQ-MG-754 probe and high kidney uptake. Other organs and the gastrointestinal tract showed very low probe uptake. Images represent organ distribution after administration of dQ-MG-754 probe (A-I), block (probe and 10fold excess of unlabeled peptide) (A-II), and DY-754 (A-III). Renal elimination was displayed by fluorescence in the bladder, which became visible directly after injection of DY-754 and dQ-MG-754 probe and persisted through the whole imaging process (B). Images were acquired with the Maestro™.

3.4. Multifactorial imaging of CCK2R expression and glycolysis

We were able to simultaneously detect the signals of both applied contrast agents, the CCK2R targeted dQ-MG-754 probe and IR800 2-DG to identify tumor metabolism in form of elevated glycolysis. Tenacity of the applied method for discrimination of the fluorescence signatures from the two probes can be found in Suppl. Fig. 6.

CCK2R expression was clearly identified by intense accumulation in the A431/CCK2R xenografts 8 h post injection, with TBRs comparable to single probe application. Likewise, a negligible accumulation was observed in A431/WT tumors. In contrast, the accumulation of IR800 2-DG was comparable in A431/CCK2R and A431/WT tumors with slowly increasing TBRs that reached their maximum at 24 h p.i. (Fig. 6A).

Looking at the individual tumors instead of mean values revealed that IR800 2-DG reached a distinct accumulation in 60% (6/10) of A431/CCK2R and in 60% (6/10) of A431/WT xenografts, defined by a TBR $>$ 3 for IR800 2-DG (Fig. 6B). The other four xenografts of each cell line would not have been detected as tumors based on IR800 2-DG, because tumor fluorescence was not particularly higher than background fluorescence. Individual analysis of dQ-MG-754 uptake, on the other hand, showed that 100% of A431/CCK2R xenografts had a TBR $>$ 3 for dQ-MG-754 and 100% of A431/WT xenografts had a TBR of $<$3 for dQ-MG-754 (Fig. 6B).

Furthermore, imaging showed differential intratumoral localization of each contrast agent (Fig. 6C).

3.5. Probe and target distribution in tumors

Ex vivo organ fluorescence as well as macroscopically scanned cryosections of tumors showed differential accumulation of the investigated contrast agents. The CCK2R targeted dQ-MG-754 probe displayed strong and homogeneously distributed fluorescence signals in explanted xenografts and cryosections of A431/CCK2R tumors, but very weak fluorescence in A431/WT tumors (Fig. 6D). Immunohistochemical validation of CCK2R expression showed a corresponding staining in A431/CCK2R tumors which was absent in A431/WT tumors.

Opposed to this, accumulation of IR800 2-DG was either heterogenous with pronounced signals in the central necrotic and perinecrotic tumor regions or very weak throughout the tumor, as seen in fluorescence analysis of explanted tumors and macroscopic scans of tumor cryosections (Fig. 6E). Histological staining of GLUT-1 receptor revealed a ubiquitous receptor expression in the vital

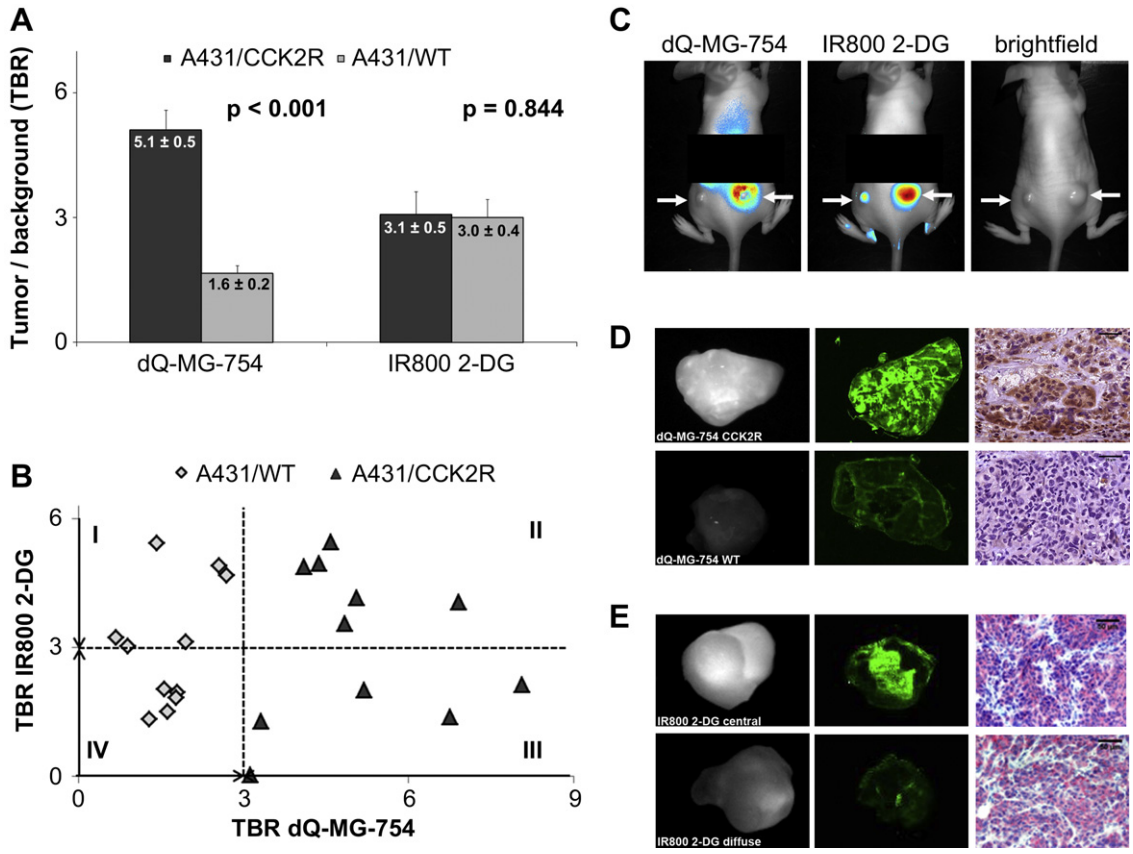

Fig. 6. Differential uptake pattern of dQ-MG-754 and IR800 2-DG probes 24 h after simultaneous administration. (A) CCK2R targeted dQ-MG-754 probe showed strong uptake only into receptor expressing tumors. IR800 2-DG probe showed moderate, but similar uptake into A431/CCK2R and A431/WT tumors. Bars display means and SEM of $n = 5$. (B) Individual subject analysis revealed that dQ-MG-754 accumulated in all A431/CCK2R tumors (quadrants II and III) and in none of the A431/WT tumors (quadrants I and IV), whereas the IR800 2-DG probe accumulated in 6/10 xenograft of either type (quadrants I and II). C) *In vivo* multispectral images shows accumulation of dQ-MG-754 in vital tumor regions of A431/CCK2R (right arrow) and centralized localization of IR800 2-DG in A431/CCK2R and A431/WT xenografts (left arrow). Images were acquired with the Maestro™. D) A431/CCK2R tumors show dQ-MG-754 fluorescence *ex vivo* (Maestro™; fluorescence displayed in grey) and in cryosections (Odyssey® 800 nm channel; fluorescence displayed in green) and were positive for CCK2R expression in immunohistochemical staining (upper row). A431/WT tumors showed weak dQ-MG-754 fluorescence *ex vivo* and in cryosections and were negative for CCK2R expression in immunohistochemical staining (lower row). E) IR800 2-DG accumulation displayed two phenotypes, independently of CCK2R expression. Either IR800 2-DG fluorescence was strong in the central region of the xenograft and weak in the vital tumor margin (upper row) or IR800 2-DG showed overall weak fluorescence in the specimen (lower row). Both cases revealed comparable GLUT-1 staining.

areas in all xenografts. Interestingly, GLUT-1 staining was also positive in xenografts that did not accumulate IR800 2-DG (Fig. 6E).

4. Discussion

Our data demonstrate that the CCK2R expressed on the surface of tumor cells can be detected together with other contrast agents addressing further tumor physiologies.

Our dQ-MG-754 probe showed a very high binding affinity, specificity and receptor mediated internalization to a cytoplasmatic location in a transfected cell model. Probe internalization also confirms that the receptor binding capability of the peptide was not impaired after coupling to the dye. Such effects are readily known to occur when coupling a relatively large dye to a small peptide molecule with limited binding sites involved in receptor binding [19].

In vivo small animal imaging further confirmed the suitability of the dQ-MG-754 probe for optical imaging. Clear tumor identification of CCK2R transfected tumors and non-transfected colorectal cancer xenografts was possible from at least 2–24 h after probe application due to relatively high tumor to background ratios. High TBRs were enabled by strong probe hydrophilicity, attained by combining a minigastrin molecule containing six glutamines at the N-terminus with the hemicyanine DY-754 with four negatively charged sulfonate groups. Our results indicate that the pronounced hydrophilicity leads to a shorter period of EPR based retention in the tumor area, caused by a reduction of plasma protein binding [32], leading to increase TBRs in comparison to the signaling of a minigastrin probe coupled to the less hydrophilic DY-676 with only two sulfonate groups [18]. Additionally, this less hydrophilic probe presented intensely high fluorescence in feces after hepatobiliary elimination. dQ-MG-754 on the other hand, showed renal elimination and no unspecific signals in the gastrointestinal tract, which is of particular importance for the prospective application in endoscopic colorectal cancer screening.

The renal elimination of the dQ-MG-754 probe was accompanied by strong kidney retention, although such retention of the respective probe components was rather inconspicuous: the hydrophilic but uncharged DOTA-coupled dQ_6-minigastrin peptide sequence was shown to manifest in low kidney uptake [27] and in our experiments the uptake of the DY-754 *per se* in the kidney was negligible (data not shown). The increased kidney retention of the probe is attributed to the combined influence of the negative charges of the dye and the hydrophilicity of the peptide. This

hypothesis is further supported by the fact that other negatively charged minigastrins also display high kidney uptake [33].

In relation to the intended application, the large kidney uptake of the probe will not impair the imaging process in intraoperative and endoscopic imaging. In addition, kidney retention is unlikely to damage kidney cells, since no ionizing radiation will be applied.

If we summarize our results related to the "dQ-MG-754" CCK2R targeted probe, it becomes clear that it combines numerous favorable properties to be considered for use in endoscopic imaging. The low molecular weight, high target affinity, long specific tumor retention, high hydrophilicity and renal elimination render the probe an excellent candidate to be used in preclinical small animal imaging and for evaluation for intraoperative and endoscopic imaging applications in the future. A promising future application for the dQ-MG-754 probe is the identification of early adenomatous legions in colorectal cancer screenings. We could basically show feasibility of this approach by successful *in vitro* and *in vivo* imaging of colorectal cancer cells physiologically expressing the CCK2R. The CCK2R has been shown to be involved in tumorigenesis, e.g. vascularization and proliferation of tumor cells in CRC, but is not expressed in the normal colon [6,8,14]. Interestingly the divergence of reported CCK2R prevalence in colorectal tumors [8,12,34,35], seems to be attributed, at least in part, to a gross underestimation of receptor expression, as this receptor is rapidly translocated to an intracellular location after ligand binding [36]. Moreover, our CCK2R targeted probe goes beyond those which are currently available for microendoscopy and fluorescence endoscopy. Their spectral properties are mainly allocated to the visible light spectrum (e.g. FITC) where extensive tissue and feces autofluorescence can overlap with the target signal [37]. At wavelengths above 700 nm signal to noise contrast is enhanced by profoundly reduced autofluorescence levels [38].

Beyond the detection of CCK2R via the dQ-MG-754 probe, a multispectral approach is also feasible. Multispectral imaging is a peculiarity of optical technologies allowing the *in vivo* detection of more than one molecular marker. The utilization of the probe IR800 2-DG, which targets elevated glycolysis and is the optical counterpart of the clinically established ^{18}F-FDG probe in nuclear medicine, revealed a distinct intratumoral accumulation pattern. The fluorescence signals of the IR800 2-DG concentrated prominently in the central region of tumors coinciding histologically with areas of necrosis as a result of an EPR dependent accumulation. Obviously, the incorporation of a dye molecule in the 2-deoxyglucose targeting moiety leads to specific opsonization processes with serum proteins [39,40], which modifies corresponding binding kinetics after crossing the leaky tumor vasculature [24].

The fact that *in vivo* fluorescence signals were indeed detected in the vital tumor area after application of the IR800 2-DG probe implies that specific binding to GLUT receptor presenting tumor cells takes place. In this context, Kovar et al. [22] and Keereweer et al. [23] showed that binding could be blocked by more than 50% with excess GLUT-1 antibody or excess 2-deoxy-D-glucose *in vitro*. Nevertheless, to our knowledge no *in vivo* blocking experiments have been published to date.

From these investigations it can be concluded that signaling of IR800 2-DG is related to both the selective binding to the GLUT-receptors as was shown by competitive approaches but also the result of the EPR effect. Hence, the IR800 2-DG probe additionally provides valuable information related to probe accessibility and perfusion of the tumor which allows us to exclude false negative probe signaling. Additionally, the proposed selective accumulation in necrotic tumor areas can provide valuable information on tumor aggressiveness and therapy planning because necrotic tumors are known to be correlated with poor prognosis [40].

Our data also demonstrate the distinct effect of the dye component used in the small molecule probes. For the CCK2R targeted dQ-MG-754 probe this means that the dedicated selection of the dye can favor pharmacokinetic and biodistribution features for intraoperative and endoscopic imaging. In contrast, the presence of a cyanine dye in GLUT targeted probes seems to shift receptor specificity towards accumulation in necrotic areas as opposed to uptake into vital GLUT-1 expressing cells in ^{18}F-FDG imaging. This is probably the reason for contradictory data in previous studies [22,24].

Complementation of imaging of tumor specific surface receptors with e.g. angiogenesis markers, glycolysis or other hallmarks of cancer can be used to predict response to anti-cancer therapy. Furthermore, analysis of tumor heterogeneity can also be a strong predictor of therapy outcome [41].

5. Conclusion

We successfully performed multifactorial *in vivo* imaging based on the detection of CCK2R overexpression in conjunction with further tumor pathologies. We showed that the CCK2R targeted dQ_6-minigastrin based NIR optical probe "dQ-MG-754" applied in this study was especially designed to unite specific high affinity binding with renal elimination and a favorable biodistribution. Besides detecting GLUT-1 receptors, the fluorescent 2-DG probe also identified areas of necrosis.

We also demonstrated that the features of the respective NIR optical probes cannot simply be extrapolated from their respective radio-conjugated counterparts. Particularly for endoscopic applications, issues in relation to biodistribution and probe elimination are of great importance beyond target affinity.

Acknowledgments

The project was supported by the German Ministry of Education and Research (BMBF, project 13N10287). We thank Beate Ziegenhardt, Susann Burgold and Yvonne Heyne for technical assistance in staining and animal handling and Brigitte Maron for logistical assistance. We thank Dr. Eckhard Birckner, Institut für Physikalische Chemie, Friedrich-Schiller University Jena, for the fluorescence lifetime measurement and Katrin Hornung for assistance in flow cytometry.

Appendix A. Supplementary data

Supplementary data related to this article can be found at http://dx.doi.org/10.1016/j.biomaterials.2013.03.073.

References

[1] van Dam GM, Themelis G, Crane LM, Harlaar NJ, Pleijhuis RG, Kelder W, et al. Intraoperative tumor-specific fluorescence imaging in ovarian cancer by folate receptor-α targeting: first in-human results. Nat Med 2011;17(10):1315–9.
[2] Terwisscha van Scheltinga AGT, van Dam GM, Nagengast WB, Ntziachristos V, Hollema H, Herek JL, et al. Intraoperative near-infrared fluorescence tumor imaging with vascular endothelial growth factor and human epidermal growth factor receptor 2 targeting antibodies. J Nucl Med 2011;52(11):1778–85.
[3] Ferlay J, Parkin DM, Steliarova-Foucher E. Estimates of cancer incidence and mortality in Europe in 2008. Eur J Cancer 2010;46(4):765–81.
[4] Jemal A, Bray F, Center MM, Ferlay J, Ward E, Forman D. Global cancer statistics. CA Cancer J Clin 2011;61(2):69–90.
[5] Mahmood U, Upadhyay R. Current and future imaging paradigms in colorectal cancer. Semin Colon Rectal Surg 2007;18(2):132–8.
[6] Smith AM, Watson SA. Gastrin and gastrin receptor activation: an early event in the adenoma-carcinoma sequence. Gut 2000;47(6):820–4.
[7] Morton M, Prendergast C, Barrett TD. Targeting gastrin for the treatment of gastric acid related disorders and pancreatic cancer. Trends Pharmacol Sci 2011;32(4):201–5.

[8] Schmitz F, Otte JM, Stechele HU, Reimann B, Banasiewicz T, Folsch UR, et al. CCK-B/gastrin receptors in human colorectal cancer. Eur J Clin Invest 2001;31(9):812–20.
[9] Imdahl A, Mantamadiotis T, Eggstein S, Farthmann EH, Baldwin GS. Expression of gastrin, gastrin/CCK-B and gastrin/CCK-C receptors in human colorectal carcinomas. J Cancer Res Clin Oncol 1995;121(11):661–6.
[10] Reubi JC, Schär J-C, Waser B. Cholecystokinin (CCK)-A and CCK-B/gastrin receptors in human tumors. Cancer Res 1997;57:1377–86.
[11] Yu HG, Tong SL, Ding YM, Ding J, Fang XM, Zhang XF, et al. Enhanced expression of cholecystokinin-2 receptor promotes the progression of colon cancer through activation of focal adhesion kinase. Int J Cancer 2006;119(12): 2724–32.
[12] Huang H, Ansorge N, Schrader H, Banasch M, Yu HG, Schmidt WE, et al. The CCK-2/gastrin splice variant receptor retaining intron 4 transactivates the COX-2 promoter in vitro. Regul Pept 2007;144(1–3):34–42.
[13] Chao C, Han X, Ives K, Park J, Kolokoltsov AA, Davey RA, et al. CCK(2) receptor expression transforms non-tumorigenic human NCM356 colonic epithelial cells into tumor forming cells. Int J Cancer 2010;15(4):864–75.
[14] Jin G, Ramanathan V, Quante M, Baik GH, Yang X, Wang SSW, et al. Inactivating cholecystokinin-2 receptor inhibits progastrin-dependent colonic crypt fission, proliferation, and colorectal cancer in mice. J Clin Invest 2009;119(9): 2691–701.
[15] Behr TM, Jenner N, Béhé M, Angerstein C, Gratz S, Raue F, et al. Radiolabeled peptides for targeting cholecystokinin-B/gastrin receptor-expressing tumors. J Nucl Med 1999;40:1029–44.
[16] Laverman P, Joosten L, Eek A, Roosenburg S, Kolenc-Peitl P, Maina T, et al. Comparative biodistribution of 12(111)In-labelled gastrin/CCK2 receptor-targeting peptides. Eur J Nucl Med Mol Imaging 2011;38(8):1410–6.
[17] Aloj L, Aurilio M, Rinaldi V, D'ambrosio L, Tesauro D, Kolenc-Peitl P, et al. Comparison of the binding and internalization properties of 12 DOTA-coupled and 111In-labelled CCK2/gastrin receptor binding peptides: a collaborative project under COST Action BM0607. Eur J Nucl Med Mol Imaging 2011;38(8): 1417–25.
[18] Laabs E, Béhé M, Kossatz S, Frank W, Kaiser WA, Hilger I. Optical imaging of CCK_2/gastrin receptor-positive tumors with a minigastrin near-infrared probe. Invest Radiol 2011;46(3):196–201.
[19] Mahmood U. Optical molecular imaging approaches in colorectal cancer. Gastroenterology 2010;138(2):419–22.
[20] Gillies RJ, Robey I, Gatenby RA. Causes and consequences of increased glucose metabolism of cancers. J Nucl Med 2008;49(Suppl. 2):24S–42S.
[21] Moreno-Sánchez R, Rodríguez-Enríquez S, Marín-Hernández A, Saavedra E. Energy metabolism in tumor cells. FEBS J 2007;274(6):1393–418.
[22] Kovar JL, Volcheck W, Sevick-Muraca E, Simpson MA, Olive DM. Characterization and performance of a near-infrared 2-deoxyglucose optical imaging agent for mouse cancer models. Anal Biochem 2009;384(2):254–62.
[23] Keereweer S, Kerrebijn JDF, Mol IM, Mieog JSD, Driel Van PBAA, Jong De RJB, et al. Optical imaging of oral squamous cell carcinoma and cervical lymph node metastasis. Head Neck 2012;34(7):1002–8.
[24] Tseng J-C, Wang Y, Banerjee P, Kung AL. Incongruity of imaging using fluorescent 2-DG conjugates compared to (18)F-FDG in preclinical cancer models. Mol Imaging Biol 2012;14(5):553–60.
[25] Aloj L, Caracó C, Panico M, Zannetti A, Vecchio Del S, Tesauro D, et al. In vitro and in vivo evaluation of 111 In-DTPAGlu-G-CCK8 for cholecystokinin-B receptor imaging. J Nucl Med 2004;45(3):485–94.
[26] Simms D, Cizdziel PE, Chomczynski P. Trizol: a new reagent for optimal single-step isolation of RNA. Focus 1993;15(4):99–102.
[27] Kolenc-Peitl P, Mansi R, Tamma M, Gmeiner-Stopar T, Sollner-Dolenc M, Waser B, et al. Highly improved metabolic stability and pharmacokinetics of indium-111-DOTA-gastrin conjugates for targeting of the gastrin receptor. J Med Chem 2011;54(8):2602–9.
[28] Limame R, Wouters A, Pauwels B, Fransen E, Peeters M, Lardon F, et al. Comparative analysis of dynamic cell viability, migration and invasion assessments by novel real-time technology and classic endpoint assays. PloS One 2012;7(10):e46536.
[29] Vermeulen PB, Gasparini G, Fox SB, Colpaert C, Marson LP, Gion M, et al. Second international consensus on the methodology and criteria of evaluation of angiogenesis quantification in solid human tumours. Eur J Cancer 2002;38(12):1564–79.
[30] Dhakal HP, Naume B, Synnestvedt M, Borgen E, Kaaresen R, Schlichting E, et al. Vascularization in primary breast carcinomas: its prognostic significance and relationship with tumor cell dissemination. Clin Cancer Res 2008;14(8): 2341–50.
[31] Fox SB, Gasparini G, Harris AL. Angiogenesis: pathological, prognostic, and growth-factor pathways and their link to trial design and anticancer drugs. Lancet Oncol 2001;2(5):278–89.
[32] Hamann FM, Brehm R, Pauli J, Grabolle M, Frank W, Kaiser WA, et al. Controlled modulation of serum protein binding and biodistribution of asymmetric cyanine dyes by variation of the number of sulfonate groups. Mol Imaging 2011;10(4):258–69.
[33] Béhé M, Kluge G, Becker W, Gotthardt M, Behr TM. Use of polyglutamic acids to reduce uptake of radiometal-labeled minigastrin in the kidneys. J Nucl Med 2005;46(6):1012–5.
[34] Upp JR, Singh P, Townsend CM, Thompson JC. Clinical significance of gastrin receptors in human colon cancers. Cancer Res 1989;49:488–92.
[35] Rehfeld JF. Gastrin and colorectal cancer: a never-ending dispute? Gastroenterology 1995;108(4):1307–10.
[36] Smith AM, Watson SA. Review article: gastrin and colorectal cancer. Aliment Pharmacol Ther 2000;14(10):1231–47.
[37] Sheth RA, Mahmood U. Optical molecular imaging and its emerging role in colorectal cancer. Am J Physiol 2010;299(4):G807–20.
[38] Frangioni J. In vivo near-infrared fluorescence imaging. Curr Opin Chem Biol 2003;7(5):626–34.
[39] Becker A, Riefke B, Ebert B, Sukowski U, Rinneberg H, Semmler W, et al. Macromolecular contrast agents for optical imaging of tumors: comparison of indotricarbocyanine-labeled human serum albumin and transferrin. Photochem Photobiol 2000;72(2):234–41.
[40] Goldshaid L, Rubinstein E, Brandis A, Segal D, Leshem N, Brenner O, et al. Novel design principles enable specific targeting of imaging and therapeutic agents to necrotic domains in breast tumors. Breast Cancer Res 2010;12(3):R29.
[41] Gillies RJ, Anderson AR, Gatenby RA, Morse DL. The biology underlying molecular imaging in oncology: from genome to anatome and back again. Clin Radiol 2010;65(7):517–21.